Seismic Tomography in Reykjanes, SW Iceland

Philippe Jousset[1], Hanna Blanck[2], Steven Franke[1,3], Malte Metz[1,4], Kristján Ágústsson[2], Arie Verdel[5], Trond Ryberg[1], Gylfi Páll Hersir[2], Cornelis Weemstra[6], David Bruhn[1], Ólafur Flovenz[2]

[1] GFZ Potsdam, Telegrafenberg, 14473 Potsdam, Germany

[2]ISOR, Iceland GeoSurvey, Reykjavik, Iceland;

[3]AWI, Neumayer Station, Antarctica

[4] Potsdam University, Germany

[5] TNO, Utrecht, the Netherlands

[6] University of Technology, Delft, the Netherlands

pjousset@gfz.potsdam.de

Keywords:
Reykjanes, seismic tomography, geothermal.

ABSTRACT

We present tomographic results obtained around geothermal reservoirs using seismic data recorded both on-land Reykjanes, SW-Iceland and offshore along Reykjanes Ridge. We gathered records from a network of 83 seismic stations (including 21 Ocean Bottom Seismometers) deployed between April 2014 and August 2015. We obtain crustal velocity images from several tomography methods. First, we used local earthquakes to perform travel time tomography. The processing includes first arrival picking of P- and S-phases using an automatic detection and picking technique based on Akaike Information Criteria. We locate earthquakes by using a non-linear localization technique, as *a priori* information for deriving a 1D velocity model. We then computed a 3D velocity model by joint inversion of each earthquake's location and velocity lateral anomalies with respect to the 1D model. Our results confirms previous models obtained in the area, with enhanced details. Second, we used ambient noise cross-correlation techniques which involve the computation of cross-correlation between seismic records. Empirical Green's functions are estimated and analyzed to derive an S-wave velocity model by surface wave tomography. Third, noise correlation theory shows that zero-offset P-wave reflectivity at selected station locations can be approximated by auto-correlating and stacking station data. With few assumptions, single-station auto-correlations provide local 1D high-resolution structural acoustic-contrast versus depth information. We show that the application of ambient noise interferometry for reflection retrieval complement well the results from both classical and noise tomography methods.

1. INTRODUCTION

The Iceland Deep Drilling Project (IDDP) is investigating on Reykjanes the economic feasibility of production of electricity in supercritical geothermal reservoirs, with higher enthalpy and lower viscosity (Dunn and Hardee, 1981, Fournier, 1999). The magnitude of enhanced productivity for the same amount of flow rate is seen to be ~10 times higher for supercritical reservoirs in comparison to conventional wells (Albertsson et al., 2003, Friðleifsson and Elders, 2000). Prior to drilling, our understanding of structural and dynamic characteristics of geothermal systems can be improved through application of advanced and/or innovative exploration technologies. Amongst geophysical exploration methods, resistivity methods are widely used in order to investigate crustal structure features of geothermal reservoirs. A combination with seismic methods is desirable (Ussher et al., 2000).

One of the most cost effective methods to deduce the crustal structure of geothermal systems is passive seismology. P- and S-wave velocities (Vp and Vs, respectively), as well as the Vp/Vs ratio vary in geothermal reservoirs due to fluid composition, rock porosity and temperature (e.g., Jousset et al., 2011). Unlike resistivity imaging, active and passive seismic techniques have however rarely been used in volcanic geothermal areas, because processing techniques were not adapted to geothermal conditions. Toomey and Foulger (1989), Foulger et al. (1995) and later Jousset et al. (2011) used local earthquake waveforms to investigate Hengill volcano complex with local seismic tomography in order to image velocity perturbations. The tomography inversion applied in these studies has successfully shown several high-velocity bodies and a low-velocity body representing a region of partial melt.

Recent advances in volcano-seismology and interferometry have introduced new processing

techniques for assessing subsurface structures and controls on fluid flow in geothermal systems. In particular, seismic tomography methods, such as surface wave tomography using seismic ambient noise can image crustal structure in terms of seismic velocity perturbations three-dimensionally (e.g. Brenguier et al., 2007; Jousset et al., 2010). In addition, Draganov et al. (2007, 2009) have shown that ambient noise cross-correlation technique are able to retrieve body waves, which provide high-resolution velocity-versus-depth as well as subsurface structural information.

We deployed a network of 30 seismic stations on Reykjanes, SW Iceland from April 2014 until August 2015 (Jousset et al., 2015; 2016; Blanck et al., 2016). The aim of this study is to collect a high quality data set that allows the computation of a 3D velocity model imaging the crustal structure, using several seismic imaging methods, i.e., travel time tomography, ambient noise tomography and reflection seismology.

2. GEOLOGY, GEOTHERMAL ACTIVITY IN THE REYKJANES PENINSULA

2.1 Geodynamic context

Iceland is located in the Northeast Atlantic where the Mid Atlantic Ridge interacts with the Iceland Hotspot. Reykjanes is located between the Western Volcanic Zone (W Iceland) and the offshore Reykjanes Ridge in the southwest of Iceland. It represents a zone of high seismic activity and recent volcanism, with a large component of regional sinistral shear movement, and with several volcanic systems, which are the westernmost in Iceland (Gudmundsson, 1987). Spreading has been active at Reykjanes since 6-7 Ma.

The peninsula is characterized by dike intrusions at depth providing the heat source for the geothermal system (Gudmundsson, 1995; Gudmundsson and Thórhallsson, 1986). The peninsula is composed of mainly young and highly permeable basaltic formations of Pleistocene age. Tholeiitic basalts range from picrite basalts (oldest) to olivine tholeiites to tholeiites (youngest) (Zindler et al., 1979). Eruptions occur in episodic intervals of roughly 1000 years. Periods of strong volcanic activity last a few hundred years and are followed by volcanically quiet periods, also lasting several hundred years. The most recent volcanic eruption in Reykjanes occurred in 1151 (Gudmundsson, 2000).

The crustal structure of Reykjanes was the topic of investigation in several geophysical and particularly seismic studies (e.g. Bjarnason et al., 1993; Menke et al., 1995; Weir et al., 2001). Surface velocities range from 2.1 to 4.2 km.s^{-1}. At increased depths, down to 4–5 km, seismic velocity increases rapidly and shows typical gradients for oceanic crust. In the surrounding ocean basin the thickness of the crust ranges from 8-11 km, which is larger than a typical oceanic crust (thickness of 7.1+/-0.8 km, e.g., White et al., 1992).

2.2 Geothermal activity in Reykjanes Peninsula

Based on high-temperature geothermal areas, magnetic anomalies and eruptive centers, the peninsula has been divided into five different volcanic systems: Hengill, Brennisteinsfjöll, Krísuvík, Svartsengi and Reykjanes (Pedersen and Grosse, 2014), to which a high temperature geothermal system is associated, and exploited. The high-temperature hydrothermal systems at Reykjanes are a result of tectonic activity, low elevation, highly permeable rock formations and high precipitation combined with high heat flow generated at the ridge axis (Gee et al., 1998). Reykjanes is located ~40 m above sea level and due to its highly porous and faulted rocks, rainwater can enter the system easily.

The Reykjanes geothermal system is located in the SW-area on the tip of the peninsula and is characterized by surface manifestations like steam vents, mud pits and warm ground. The geothermal system is a seawater-recharged hydrothermal system and interacts highly with the oceanic crust. A power plant has been operating at this site since 2006 with an efficiency of 100 MWe. Two shallow wells at depths of 1225 m and 960 m produce saturated steam from the steam cap with a thermal capacity of ~2700 kJ/kg (Fridriksson et al., 2010). At a depth of more than 1 km, temperatures range from 275° to 310°C and fluid consists of chemically modified seawater with components of magmatic gases due to the basaltic host rocks (Arnórsson, 1978). Increasing surface activity in the area of the reservoir seems to be linked with an increase in seismic activity. The energy production and exploitation of geothermal reservoirs in Reykjanes is rather limited and expansion requires further exploration. As drilling wells are a major matter of expense in geothermal reservoir exploration, efforts to perform geophysical exploration are fully justified.

3. TRAVEL TIME TOMOGRAPHY AT REYKJANES

3.1 Seismic activity at Reykjanes

Seismic activity in Iceland is occurring in the Tjörnes Fracture Zone, in the South Iceland Seismic Zone (the majority at Hengill triple junction) and in Reykjanes Peninsula (Jakobsdóttir, 2008). In Reykjanes, the seismic activity occur at potential active area like volcanoes, in the surrounding of geothermal exploited areas (induced seismicity) and in the Reykjanes Ridge. Big earthquake swarms may occur all along the Peninsula (Jakobsdóttir, 2008). Furthermore, rather higher magnitude events also occur, e.g., an Mw 5.2 event located at Sveifluháls, near Kleifarvatn on 23 August 2003. The vast majority (90%) of detected earthquakes occur at depth of ~1.5 km and are normal faulting or strike-slip events (Klein et al., 1977). The high abundance of local earthquakes in Reykjanes is very beneficial for a successful and reliable tomographic inversion.

3.2 Overview of seismic travel-time tomography method

Seismic tomography is a geophysical technique for imaging the three-dimensional distribution of physical properties like elasticity, anisotropic parameters and density in the subsurface (Aki and Lee, 1976). As a result, it is possible to analyse the subsurface in terms of lithology, temperature, fracturing and fluid content. The first local earthquake tomography studies were carried out by Kissling (1988).

The principle of the method is based on the analysis of ray-paths of (typically) arrival times (or attenuation measurements), which are crossing each other in the crust. In a mathematically simplified way, this represents a system of linear equations. The biggest challenge is that (heterogeneous) structures within the volume and ray-paths crossing the volume interact with each other and are thus themselves part of the problem, making seismic tomography a non-linear inverse problem (Evans et al., 1994). In practice, this inversion problem can be linearized and the solution can be constrained by *a priori* information. The resolution of the resulting image is strongly dependent on the distribution and amount of ray-paths within the volume.

3.3 Seismological Network and data acquisition

We deployed 30 seismic stations (20 Trillium Compact Broadband seismometers (BB) and 10 short-period Mark L-4C seismometers (SP)) and we used existing networks (Blanck et al., 2016). Each station comprises a seismometer, a data logger, a GPS unit and a power source (Figure 1). The position of each seismometer was determined with a DGPS (Differential GPS) system (Trimble), which provides an accuracy of less than a meter. The orientation of the seismometers were determined using a fiber-optic gyrocompass, which gives azimuth with an accuracy of about 0.1 degrees. The IMAGE network comprises DATA-CUBE data loggers (distributed by Omnirecs): unlike regular systems (e.g. REFTEK) they are small, light, waterproof and are extremely low power consuming data logger with an integrated flash. Just 30 Ah battery were used as source of power, and could last for 3 months. The sampling rate for all stations is 200 Hz. Seismic data was stored in raw format on 15 GB flash memory. The data were extracted locally every 71 days and transferred from ÍSOR headquarters in Reykjavík to GFZ-Potsdam via ftp-server.

3.4 Data Processing

We analyzed the records using an integrated tool (Seismotool ©) written in Matlab by Jousset (2006) and with seismcomp (Blanck et al., 2016). Seismotool enables us to process passive seismic data recorded on networks and performs several tasks automatically:

* read data according to the file format at all stations;
* perform calibration of records according to the instrument response (stored in a database).
* perform event detection using a STA/LTA (Short Term Average / Long Term Average) technique on the envelope of the signals;
* classify events according to the number of stations at which the detection flag was raised.
* analyze waveforms for P and S manual or automatic picking.

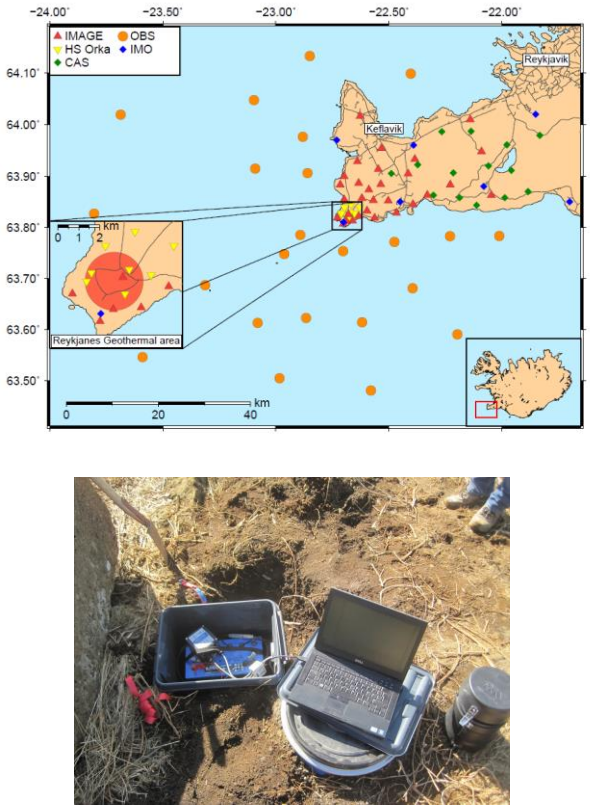

Figure 1: Seismic network used in this study and example of deployment of a seismic station of the IMAGE network (see Blanck et al., 2016 for details).

Details of each step of the processing are given in Franke (2015). Visual inspection of the data can be performed for picking arrival times and associated error for both P- and S-phases wherever possible. In order to support the accuracy of P- and S-phase picking, we use the Akaike Information Criterion, (Akaike, 1973). The criteria defines the onset of the wave as the point where the AIC has a minimum value (Jousset et al., 2011). Instead of just selecting one value as a phase arrival, we place two picking values in the interval where we locate the phase arrival. The time range defines the picking error for that phase. This criteria allows us to weight P- and S- wave's picks and consider better high quality events, in order to reduce potential errors in the 1D and 3D tomography inversion. An automatic picking procedure for the AIC was tested and applied. Misplaced and missing phases were corrected using visual projection of the Wadati diagram, in which S arrival time (or S-P arrival time) are plotted against P arrival time (Wadati, 1933, Chaterjee et al., 1985, Figure 2).

A joint inversion of arrival times for hypocenter locations and velocity structure was first performed one-dimensionally and used as input for the same procedure in 3D. *A priori* information about the subsurface and estimated hypocenter locations contribute to a better and more reliable result from the tomographic inversion. A preliminary localization was performed with a constant velocity model by a grid search non-linear inversion in which travel times are computed (Jousset et al., 2011). This localization served as *a priori* information for the 1D velocity inversions. For our study, we used Vp of 4 km/s and Vp/Vs ratio of 1.76 (Franke, 2015).

The minimal 1D velocity model of the subsurface consists in finding the best model (in terms of vertical position, amount and thickness of seismic velocity layers). The quality of the final model is expressed by the minimal difference (misfit) of observed and calculated travel times, in the least square sense. We used VELEST (Kissling et al., 1994). In the first step, the forward problem is solved by ray tracing from event source to receiver location and the ray paths through the 1D model are computed. Then, the damped least squares matrix is computed and the corresponding inverse problem is solved by full inversion of the matrix. Hypocentre locations, model and station corrections are adjusted iteratively.

For the 3D model inversion, we used SIMULPS (Thurber, 1983; Eberhart-Phillips, 1990) in which an iterative, damped least-squares method inverts seismic arrival times and computes earthquake locations in a 3D velocity field (Evans et al., 1994). The parametrization is defined by node values in a -D grid were Vp and Vp/Vs values are assumed to follow trilinear functions (Charlety et al., 2006). The forward problem is solved by approximate 3D ray-tracing (Thurber, 1983) and pseudo-bending (Um and Thurber, 1987). We use the 1D velocity model derived from our own data from VELEST as *a priori* information. In SIMULPS the damping parameter is chosen by examining a plot of the data misfit against the model variance, the trade-off curve. We chose a damping value of 25 and 30, which produces a good compromise between data misfit and model variance.

3.5 Results

We present partial results of our processing of seismic data. We focus on a recording period of 9 months, from March to December 2014 at Reykjanes.

3.5.1 Seismic activity

Among the 2000 detected events, we focus here on 712 local earthquakes (and correspondingly 11 125 P- and S-phase couples and travel times) and we picked P- and S- wave arrival times manually. A minimum of 6 stations where P- and S-phases respectively are clearly detected and in accordance with the general alignment in the Wadati diagram and a corresponding reasonable Vp/Vs ratio. The average picking error for P-waves is 0.018 s and 0.054 for S-waves. From the Wadati diagram (Figure 2), we inferred a Vp/Vs ratio of 1.76+/-0.06, which is in the range of previous studies.

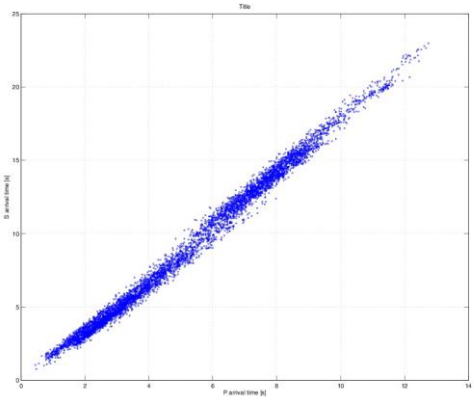

Figure 2: Wadati diagram of all 720 earthquakes with P- and S- wave's arrival times from April 2014 until December 2014. Our analysis lead to Vp/Vs = 1.76+/-0.06.

3.5.2 1D velocity model tomography

The 1D velocity model is parametrized in horizontal layers of constant P-wave velocity. The first 4 km (from 1 km elevation to 3 km depth) have 1 km thick layers. Then from 3 to 5 km depth, 5 to 8 km and 8 to 12 km, layers are 2 km, 3 km and 4 km thick, respectively. Many tests with a different combination of initial parameters with respect to Vp a priori values, gradients and Vp/Vs ratios have been performed in order to inverse for the best 1D velocity model (Franke, 2015).

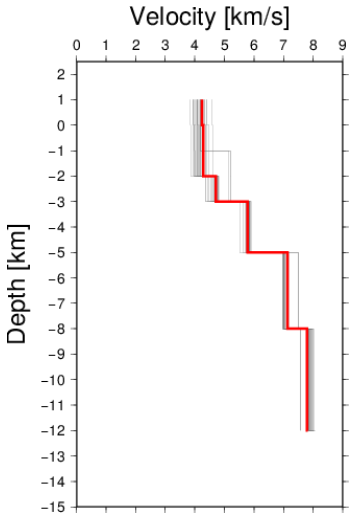

Figure 3: Minimum 1D velocity model obtained from the many tests performed with 377 earthquakes from April to December 2014.

Figure 3 shows the results for the least RMS of all our inversions. The model shows an almost constant velocity structure down to 2 km depth of 4.24 – 4.28

km/s. The velocity structure increases in large steps from 4.71 to 7.14 km/s between 3 and 8 km depth.

Hypocentre localizations are also given as an output of the inversion (Figure 4). Apart from a few outliers, most events are located in a west-southwest to east-northeast striking line. Offshore events are located in a dense cluster in the west of the Reykjanes geothermal reservoir. An azimuthal gap criteria was applied on earthquake location with respect to the station locations. The number of events usable decreased dramatically from 712 to 377 (from 11 125 to 4 818 P- and S- phase readings) prior to 1D inversion. The 1D tomography inversion relocated 86 events outside of the network reducing further the events number from 377 to 191. However, by performing the inversion on the base of these 191 earthquakes, the structure is similar to the one shown in Figure 3 (with 377 earthquakes). The 1D velocity structure derived by 1D tomography (Figure 3) is in agreement with other models derived for SW Iceland (e.g., Bjarnason et al., 1993).

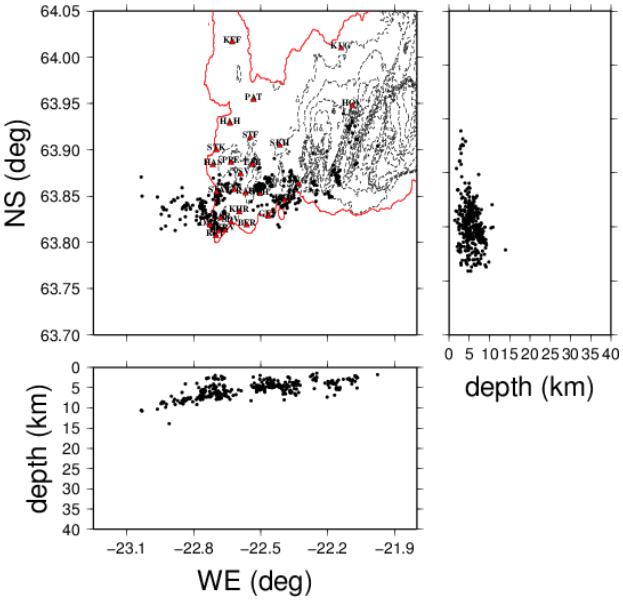

Figure 4: Earthquake locations deduced from the minimum 1D velocity model obtained from the many tests performed with 377 earthquakes from April to December 2014.

3.5.3 3D velocity model tomography

We performed many 3D inversion tests according to the results of the 1D tomography. In accordance with the trade-off curve (not shown), damping was set to 25. The final RMS value for the best inversion was 0.142. Figure 5 displays ray paths from the 377 earthquakes recorded at 26 stations. The ray paths density is a good proxy for the resolution estimation. Areas of reduced ray coverage correspond to areas of low resolution.

Figure 6 shows two slices at two different depths and an EW cross-section of the 3D tomography results. The crosses in the map views and cross sections indicate the points of parametrization of the lateral and vertical space. Intense colours indicate well resolved areas. Spaces with weak colour reveal a lack of ray-paths coverage and are poorly resolved. Fields of no colour are not well resolved at all. Earthquake locations are represented by red dots.

A high velocity anomaly in the southwest tip of Reykjanes is visible at all depths. The anomaly shows the highest absolute P-wave of ~8.5 km/s velocity at 5 – 7 km depths and decreases at shallower depth. At a depth of 0.5 km the area shows a P-wave velocity ~5.5 km/s. Vp decreases rapidly to the northeast by a magnitude of 2 – 2.5 km/s. At depths of 2.5 to 4.0 km a low velocity anomaly is clearly imaged to the northeast of the high velocity anomaly. This feature is also present at further depth. The lack of resolution however, makes it difficult to get an idea of the whole picture at these depths. A further high velocity anomaly is located at -22.475°W/63.85°N. It is rudimentary visible at a depth 0.5 km and can be monitored down to 3.5 km depth.

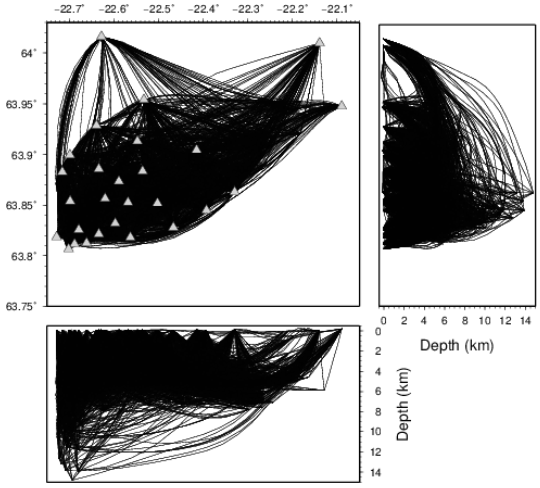

Figure 5: Ray path of the 377 earthquakes of this study to the 26 stations (triangles) at the surface.

The high velocity body in the southwest can be seen in all tests we have performed. In particular, we performed an inversion with a damping raised from 30 to 120. The high velocity anomaly is still present, although not as dominant as when damping is 30. The low velocity anomaly detected northeast of the high velocity body is not visible clearly as the high velocity body but still present. We interpret the results of this test as a confirmation of the robustness of our results. In addition, the preliminary 3D inversion with 2000 earthquakes and including picks from the OBS data confirms this high Vp anomaly in the south-west of Reykjanes and reveal its extension along the ridge.

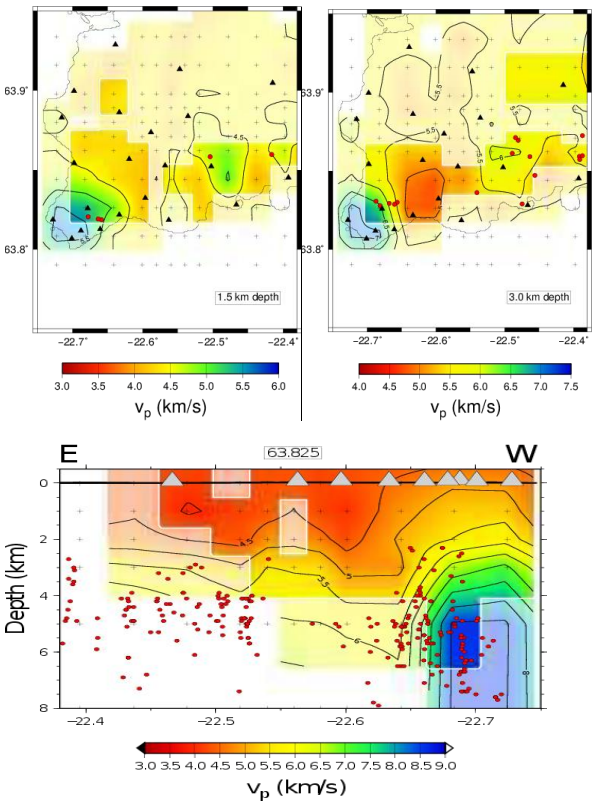

Figure 6: (top) 2 slices (bottom) cross-section, showing the results of the 3D tomography performed with 377 earthquakes from April to December 2014.

Figure 6 shows also an EW cross-section of the results. The profile crosses the high velocity body to the west and resolves the velocity structure down to a depth of 6 km. Earthquake hypocenters are concentrated in an area between 63.90 N and 63.85 N in a depth range of 3 – 7 km. The full high velocity anomaly can be imaged and reveals P-wave velocities ranging from -4.5 – 8.5 km/s. The upper 4 km of the high velocity body are particularly well resolved. Compared to the northern part of the cross section, we clearly see an increased velocity gradient around the high velocity body.

3.6 Tentative interpretation

Due to the reduced station number and earthquake number, only a partial interpretation is possible. Tryggvason et al. (2002) detected a high P-wave velocity anomaly at 6-7 km depth at the same area. We find this high velocity anomaly in the southwestern tip of Reykjanes, which correlates with the location of the Reykjanes geothermal area. High P-wave velocities can be explained by a variety of features. In this particular geological setting however, fluid saturation can be one factor for increased P-wave velocities. The reservoir is located closely to the sea and as described earlier, generates its hydrothermal fluids through seawater. However, geodetic observations reveal subsidence of the ground in that area. This suggests that the rate of refill of seawater into the reservoir is not very high. Another factor that increases Vp, can be a magma intrusion of denser material. This would correlate with recent volcanic activity at Reykjanes, which is also in agreement with a high heat flux.

4. REYKJANES AMBIENT NOISE SURFACE WAVE TOMOGRAPHY

It has been shown that ambient seismic noise is able to produce images of the sub-surface, by using cross-correlation techniques and can further be used for structural analysis with tomographic methods (e.g., Ryberg et al., 2016).

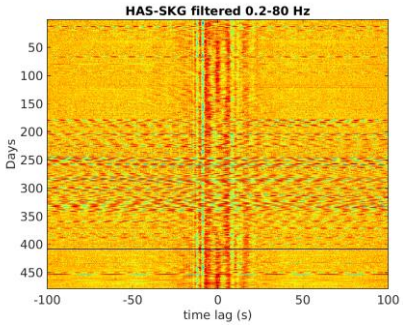

Figure 7: Daily cross-correlations computed for more than a year of records at stations HAS and SKG. Note the stability of the Green function, except during storms in winter months (e.g., days ~250 to ~350).

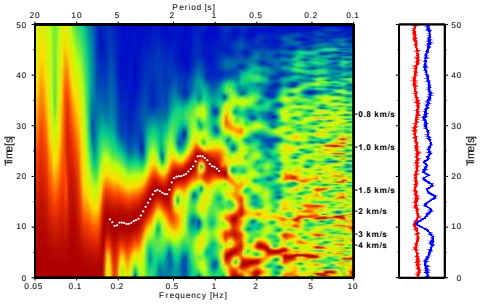

Figure 8: Causal and acausal parts of the cross-correlation function (top trace) for the station pair GEV-KUG (distance ~26 km). Travel time (group velocity) picks are indicated by white circles.

We performed cross-correlation of ambient noise using the high quality data of our network to retrieve the empirical Green's functions. The observed cross-correlations are generally dominated by surface waves. The proximity of the Atlantic Ocean and the large and intense storms produce strong ambient noise, making this technique particularly efficient in Iceland (Figure 7). We stacked daily cross-correlations between the broadband sensors, and obtained 465 cross-correlation functions (pair of stations). The group velocities were estimated using a multiple-filter, frequency-time analysis (Dziewonski et al., 1969). We picked manually the dispersion curves on the vertical component only. All station pairs show clearly visible

Rayleigh wave dispersion curves in the typical period range between 5 and 1 s (Figure 8).

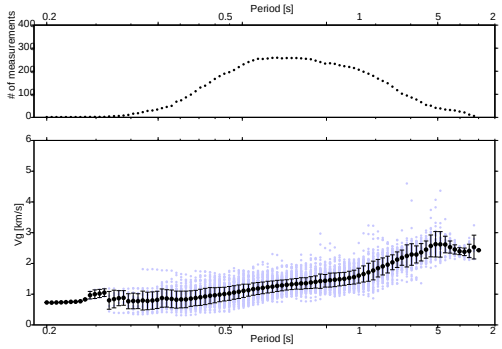

Figure 9: Rayleigh wave group velocity measurements in the study area. (Bottom) grey dots represent individual group velocity determinations, black dots show the average dispersion curve with their respective standard deviations. The top panel shows the number of measurements as a function of signal period.

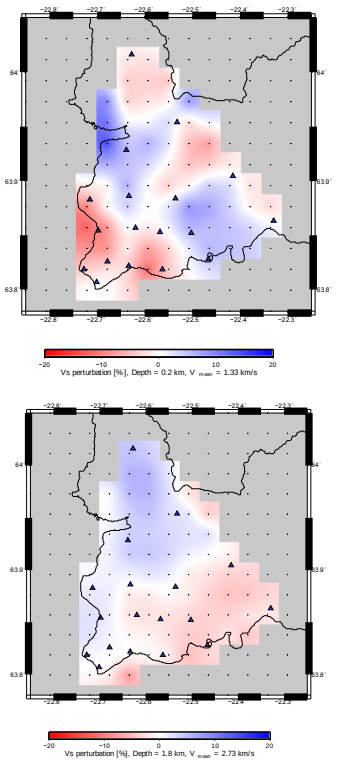

Figure 10: Preliminary results of the ambient noise tomography at Reykjanes for 2 depth-slices. (Top) 200 m depth. Note the higher Vs anomaly at the tip of Reykjanes and at the location of Svartsengi. (Bottom) 1800 m depth. Note the lower Vs anomaly at the location of the ridge.

For each period, we derived group velocity maps from the group velocities (or travel time picks of Rayleigh waves) between stations, by applying the FMST (Fast Marching Surface Tomography) package by Rawlinson and Sambridge (2005). Then, although the inversion of group velocity dispersion curves for S-wave velocity (Vs) depth functions is not trivial (given the highly non-unique character of this procedure), we used the iterative linearized least-square inversion procedure of Herrmann and Ammon (2004). Figure 9 shows preliminary results using this method. Further validation in under process.

5. REYKJANES AMBIENT NOISE REFLECTION INTERFEROMETRY

In order to complement our results and to image P-wave reflections underneath Reykjanes Peninsula, we applied Ambient-Noise Seismic Interferometry (ANSI). For that purpose, we processed the continuous records to retrieve primary reflected body waves (P-waves), which could provide high-resolution velocity/depth functions, as well as subsurface structural information. In general, surface wave noise is much stronger than body-wave noise that is required for producing reflection images. There is, however, evidence that reflections can also be retrieved (Draganov et al., 2007, 2009).

In his pioneering 'daylight imaging' paper, Claerbout (1968) already described the ANSI principle for plane waves in a plane-layered earth. His early results imply that the P-wave reflectivity recorded at zero source-receiver offset can be approximated by auto-correlating and stacking continuous transmission data over long periods of time, typically days or weeks. It is thereby assumed that the lateral velocity variations in the subsurface are relatively small and that uncorrelated noise sources illuminate the subsurface from below. Under these assumptions, single-station auto-correlations may provide local 1D structural acoustic-contrast versus depth information. When repeating the auto-correlation method for a line or grid of seismometers, a sparse 2D resp. 3D image of seismic reflectivity emerges. The resolution of such a structural image depends on the frequency content of the noise sources. And if repeated for other periods of time, time-lapse variations of seismic reflection - amplitudes and – times may additionally be retrieved (Weemstra et al., 2016).

Here, we only show a data processing result obtained from long duration continuous data recordings from just one broadband seismometer and compare that result to ad-hoc seismic trace inversions for velocity and depth (Verdel at al., 2016).

In Figure 11, an example is shown of a zero-offset reflectivity result (leftmost trace) in the frequency band 3-8 Hz for a single broadband seismometer, station LFE, located approximately 7 km from the nearest coastline (Figure 1), after stacking 40 consecutive days of auto-correlated recorded noise (vertical component of particle velocity only). The second trace from the left shows the same result but after spectral whitening such that it can be easily compared with modelled reflectivity scenarios. It can be seen from a comparison with the third trace from the left that a velocity-depth model with a thick

shallow high velocity layer (Model 3) far better matches the LFE station data than the results from the other two models shown (see the two rightmost panels and the corresponding velocity models plotted on top of those). This type of velocity-depth information can be considered a useful local refinement of results from tomographic inversion of surface waves.

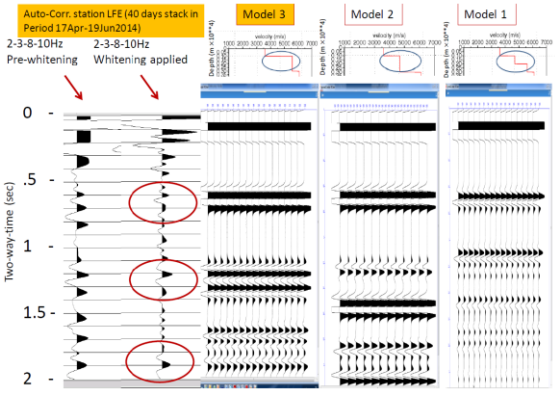

Figure 11: ANSI-processed reflectivity for station LFE (two traces on left) and modelled reflectivity (TNO, 2016).

By applying the ANSI method to all stations on Reykjanes, a sparse map of zero-offset P-wave reflectivity in the upper few kilometres of the Reykjanes area is created. This approach is expected to address the question raised by geothermal field operator HS Orka: "Down to which depth do our geothermal reservoirs extend?" Ambient noise data recorded by the entire on-land broadband seismometer network is currently being analysed in detail. If the auto-correlation results justify additional processing efforts, the following step would be to cross-correlate station-pairs in this seismometer network for the production of virtual source panels that contain P-wave reflections. This has the potential of further reducing uncertainties in, for geothermal exploitation, relevant subsurface parameters, such as the spatial distribution of seismic velocity jumps.

6. CONCLUSIONS AND CURRENT WORK

A crustal seismic P-wave velocity model for Reykjanes, SW Iceland, has been derived by 3D seismic travel time tomography from local earthquakes. More than 2000 seismic events were recorded from April 2014 to August 2015 by our network. We presented here partial tomographic analysis on the basis of sub-set of 712 local earthquakes and the on-land seismic network. 377 earthquakes were localized within the area of the seismic network and were selected to compute a minimum 1D velocity model for the region. This model served as initial model for a non-linear inversion of seismic travel times to obtain the 3D velocity structure. The best fitting 3D velocity model reveals a high velocity anomaly located in the southwest tip of Reykjanes correlating with Reykjanes geothermal field. A second high velocity body corresponds to the location of Eldvörp geothermal field.

We also performed surface wave tomography with a subset of the network. Our preliminary results reveal an S-wave velocity structure compatible with lower S-wave velocities in the Ridge.

In order to improve the results of seismic tomography, more ray paths are required. In a first attempt to step beyond the results of the present study, we obtained preliminary tomography results by using more than 2000 earthquakes and stations from the Icelandic SIL (belonging to the Icelandic Meteorological Office, IMO) permanent network, and from ocean-bottom-seismometers (OBS) deployed (in cooperation with the Alfred-Wegener-Institute for Polar and Marine Research. The results confirm the main obtained result of this study, i.e., a high Vp anomaly starting at the tip of the Peninsula and extending towards the ridge.

In general, relating seismic observations with rock properties, especially in volcanic areas, is not trivial. There are certain rules one could apply when interpreting tomographic images, but they have to be considered with care, due to the complexity and non-uniqueness in the context of seismic velocity or attenuation and rock parameters. In many seismic tomography analyses a decrease of P- and S-wave velocity is correlated with increasing temperature. The magnitude of this effect is expressed rather weakly, but increases abruptly when temperature exceeds a certain threshold and the considered volume is composed of partially molten or completely molten material. This applies especially to the behavior of S-waves. Fluid saturation generally induces higher P-wave velocity Negative P-wave velocity anomalies (lower relative Vp) are associated with changes in lithology, crystal structure, crack density and the presence of different phases (Iyer, 1992; Mavko, 1980; Mavko and Nur, 1978). Rock properties derived from seismic observations are difficult to relate because several characteristics affect variations in seismic features in the same way. The classic parameters under investigation in seismic tomography studies are velocity (Vp and Vs) and attenuation (QP and QS) and their rations Vp/Vs and QP/QS. Thus, the inherent non-uniqueness of tomography interpretations requires some form of *a priori* or additional information to constrain possible interpretation options (Lees, 2007). Our future work will incorporate those results into a updated structural model of Reykjanes, which will also be eventually be constraint with a resistivity model. Additionally, a fibre optic cable was deployed on Reykjanes. One aim is to monitor the vertical heat distribution in a borehole and the other approach is to register signals on a lateral profile (Jousset et al., 2016; Reinsch et al., 2016).

ACKNOWLEDGEMENTS

H.S. Orka gave access to the geothermal field in Reykjanes. The Czech Academy of Science (Czech Republic) and the Iceland Meteorological Office (Iceland) provided us with seismic data. Instruments for the IMAGE project were provided by the GIPP

(Geophysical instrumental Pool of Potsdam) and the DEPAS (Deutsche Geräte Pool für Amphibische Seismologie). We would like also to thank the Iceland Coast Guard for the OBS recovery. Mykola Khyzhnyak, Sigrún Tómasdóttir, Sif Pétursdóttir, Guðrún Ósk Sæmundsdóttir performed most of the picking work. The research leading to these results has received funding from the EC Seventh Framework Programme under grant agreement No. 608553 (Project IMAGE).

REFERENCES

Akaike, H. (1973). Information theory and an extension of the maximum likelihood principle. In Budapest Akademiai Kiado, pages 181–267.

Aki, K. and Lee, W. (1976). Determination of the three-dimensional velocity anomalies under a seismic array using first p arrival times from local earthquakes 1. A homogeneous initial model. J. Geophys. Res., 81:4381–4399.

Albertsson, A., Bjarnason, J., Gunnarsson, T., Ballzus, C., and Ingason, K. (2003). Part III: Fluid Handling and Evaluation. In: Iceland Deep Drilling Project, Feasibility Report. (Ed.) G.Ó. Friðleifsson. Okustofnun Report OS-2003-007, page 33p.

Árnason, K., Karlsdóttir, R., Eysteinsson, H., Flóvenz, Ó.G. and Gudlaugsson, S.Th. (2000). The resistivity structure of high-temperature geothermal systems in Iceland. Proceedings of the World Geothermal Congress 2000, Kyushu-Tohoku, Japan, 923–928.

Arnórsson, S. (1978). Major element chemistry of the geothermal sea-water at Reykjanes and Svartsengi, Iceland. Mineralogical Magazine, 42:209–220.

Bjarnason, I., Menke, W., Flovenz, D., and Caress, D. (1993). Tomographic image of the spreading center in south Iceland. J. Geophys. Res., 98:6607–6622.

Blanck, H., Jousset, P., Ágústsson, K., Hersir, G.P. and Flóvenz Ó.G. (2016). Analysis of seismological data on Reykjanes peninsula, Iceland. Extended abstract EGC, Strasbourg, September 2016.

Brenguier, F., Campillo, N., Nercessian, A., and Ferrazzini, V. (2007). 3D surface wave tomography of the Piton de la Fournaise volcano using seismic noise correlations. Geophysical Research Letters, 34:L02305, doi:10.1029/2006GL028586.

Charlety, J., Cuenot, N., Dorbath, C., and Dorbath, L. (2006). Tomographic study of the seismic velocity at the Soultz-sous-Forêts EGS/HDR site. Geothermics, 35:532–543.

Chaterjee, S., Pitt, A., and Iyer, H. (1985). Vp/Vs ratios in the Yellowstone National Park Region, Wyoming. J. Volcanol. Geotherm. Res., 26:213–230.

Claerbout, J. F., 1968, Synthesis of a layered medium from its acoustic transmission response: Geophysics, 33, 264–269, doi: 10.1190/1.1439927.

Dziewonski, S. Bloch, M. Landisman (1969). A technique for the analysis of transient seismic signals. Bull. Seismol. Soc. Am., 59 (1), 427–444

Dunn, J. and Hardee, H. (1981). Superconvecting geothermal zones. J. of Volcanology and Geothermal Res., 11:189–201.

Draganov, D., Wapenaar,K., Mulder, W., Singer, J., and Verdel, A.. (2007). Retrieval of reflections from seismic background-noise measurements: Geophysical Research Letters, 34, L04305, doi: 10.1029/2006GL028735.

Draganov, D., Campman, X., Thorbecke, J., Verdel, A., and Wapenaar, K. (2009). Reflection images from ambient seismic noise, *Geophysics*, Vol. 74, no. 5, A63-A67, doi: 10.1190/1.3193529.

Eberhart-Phillips, D. (1990). Three-dimensional P and S velocity structure in the Coalinga region, California. J. Geophys. Res., 95:15343–15363.

Evans, J., Eberhart-Phillips, D., and Thurber, C. H. (1994). User's Manual for SIMULPS12 for imaging Vp and Vp/Vs. A Derivative of the Thurber Tomographic Inversion SIMUL3 for Local Earthquakes and Explosions. US Geological Survey Open File Report OFR 94-431, page p. 101.

Eysteinsson, H. (2000). Evaluation and gravity changes at geothermal fields on the Reykjanes Peninsula,SW Iceland. Proceedings World Geothermal Congress 2000, pages 559–564.

Foulger, G., Miller, A., Julian, B., and Evans, J. (1995). Three-dimensional Vp and Vp/Vs, structure of the Hengill Triple Junction and geothermal area, Iceland and the repeatability of tomographic inversion. Geophysical Research Letters, 22 (10):1309–1312.

Fournier, R. (1999). Hydrothermal processes related to movement of fluid from plastic into brittle rock in the magmatic-epithermal. Economic Geology, 94:1193–1211.

Franke, S. (2015). Local seismic travel time tomography on geothermal reservoirs at Reykjanes, Iceland. M.Sc. dissertation, University of Copenhagen/GFZ Potsdam, 90 pp.

Fridriksson, T., Oladottir, A., Jonsson, P., and Eyjolfsdottir, E. (2010). The Response of the Reykjanes Geothermal System to 100 MWe Power Production: Fluid Chemistry and Surface Activity. Proceedings World Geothermal Congress 2010, pages 1–7.

Friðleifsson, G. and Elders, W. (2000). The Iceland Deep Drilling Project (IDDP) – 10 years later – Still on Opportunity for an International Collaboration. Proc. World Geothermal Congress 2010, page paper 3901.

Gee, M., Thirlwall, M., Taylor, R., Lowry, D., and Murton, B. (1998). Crustal Processes: Major Controls on Reykjanes Peninsula Lava Chemistry, SW Iceland. Journal of Petrology, 39:819–839.

Gudmundsson, A. (1987). Geometry, formation and development of tectonic fractures on the Reykjanes Peninsula, southwest Iceland. Tectonophysics, 139:295–308.

Gudmundsson, A. (1995). Ocean-ridge discontinuities in Iceland. J. Geol. Soc., 152:1011–1015.

Gudmundsson, A. (2000). Dynamics of volcanic systems in Iceland: example of tectonism and volcanic at juxtaposed hot spot and mid-ocean ridge systems. Ann. Rev. Earth. Planet. Sci., 28:107–140.

Gudmundsson, J. and Thórhallsson, S. (1986). The Svartsengi Reservoir in Iceland. Geothermics, 15:3–16.

Herrmann, R.B. and C.J. Ammon (2004) Surface waves, receiver functions and crustal structure. Computer Programs in seismology, version 3.30, Saint Louis University.http://www.eas.slu.edu/People/RBHerrmann/CPS330.html.

Iyer, H. (1992). Seismological detection and delineation of magma chambers: present status with emphasis on the western USA. In: Gasparini, P., Scarpa, R., Aki, K. (Eds.). Volcanic Seismology. Springer-Verlag, Berlin, pages 299–338.

Jakobsdóttir, S. (2008). Seismicity in Iceland: 1994-2007. Jökull, 58:75–100.

Jousset, P. (2006). Sismologie large bande: Méthodologie et applications: apport en géothermie haute enthalpie à Bouillante, Guadeloupe. Rapport BRGM RP-54701-FR, page 119 pp.

Jousset, P., Bitri, A., Loiseau, J., and Bouchot, V. (2010). Seismic ambient noise study at Bouillante geothermal system, French Antilles. In: Geophysical Research Abstracts, EGU General Assembly 2010, pages p. EGU2010–5305.

Jousset, P., Haberland, C., Bauer, K., and Arnason, K. (2011). Hengill geothermal volcanic complex (Iceland) characterized by integrated geophysical observations. Geothermics, 40:1–24.

Jousset, P., K., Ágústsson, A., Verdel, H., Blanck, S., Franke, S., Specht, S., Stefánsson, H.,Tryggvason, K.,Erbas, F., Deon, Ö., Erlendsson, E., Guðnason, G. Hersir, S. Halldórsdóttir, C. Weemstra, D., Bruhn, Ó., Flovenz, and Ó., Friðleifsson (2015). Imaging hydrothermal systems associated with oceanic ridge: ambient noise and travel-time tomography in the Reykjanes high-temperature area, SW-Iceland. Geophysical Research Abstracts Vol. 17, EGU2015-13904, 2015, EGU General Assembly 2015.

Jousset, P., Verdel, A., Ágústsson, K., Blanck, H., Franke, S., Metz, M., Ryberg, T., Weemstra, C., Hersir, G., and Bruhn, D. (2016). Seismic tomography and ambient noise reflection interferometry on Reykjanes, SW Iceland. Geophysical Research Abstracts Vol. 18, Vol. 18, EGU2016-13795, 2016, EGU General Assembly 2016.

Kissling, E. (1988). Geotomography with local earthquake data. Reviews of Geophysics, 26 (4):659–698.

Kissling, E., Ellsworth, W., Eberhart-Phillips, D., and Kradolfer, U. (1994). Initial reference models in seismic tomography. J. Geophys. Res, 99:19635–19646.

Klein F., P. Einarsson, and M. Wyss (1977). The Reykjanes Peninsula, Iceland, earthquake swarm of September 1972 and its tectnonic significance. J. Geophys. Res. 82: 865-888.

Lees, J. (2007). Seismic tomography of magmatic systems. Journal of Volcanology and Geothermal Research, 167:37–56.

Mavko, G. (1980). Velocity and attenuation in partially molten rocks. J. Geophys. Res., 85 (B10):5173–5189.

Menke, W., Levin, V., and Sethi, R. (1995). Seismic attenuation in the crust at the mid-Atlantic boundary in south-west Iceland. Geophys. J. Int., 122:175–185.

Pedersen, G. and Grosse, P. (2014). Morphometry of subaerial shield volcanoes and glaciovolcanoes from Reykjanes Peninsula, Iceland: Effects of eruption environment. Journal of Volcanology and Geothermal Research, 282:115–133.

Rawlinson, N. and M., Sambridge (2005). The fast marching method: an effective tool for tomographic imaging and tracking multiple phases in complex layered media. Explor. Geophys., 36, 341–350.

Reinsch, T., P., Jousset, J., Henninges, H. Blanck (2016). Distributed Acoustic Sensing Technology in Magmatic Geothermal Areas – First Results from a Survey in Iceland. Extended abstract EGC, Strasbourg, September 2016.

Ryberg, T., Muksin, U. and K., Bauer (2016). Ambient seismic noise tomography reveals a hidden caldera and its relation to the Tarutung pull-apart basin at the Sumatran Fault Zone, Indonesia. J. Volcanol. Geotherm. Res. 321, 73-84.

Thurber, C. (1983). Earthquake locations and three-dimensional crustal structure in the Coyote Lake area, central California. J. Geophys. Res., 88:8226–8236.

Toomey, D. and Foulger, G. (1989). Tomographic inversion of local earthquake data from the Hengill-Grensdalur central volcano. J. Geophys. Res., 94:497–517.

Tryggvason, A., Ragnvaldsson, S. T., and Flóvenz, Ó. (2002). Three-dimensional imaging of the p- and s-wave velocity structure and earthquake locations beneath southwest Iceland. Geophys. J. Int., 151:848–866.

Um, J. and Thurber, C. (1987). A fast algorithm for two-point seismic ray tracing. Bulletin of the Seismological Society of America, 77 (3):972–986.

Ussher, G., Harvey, C., Johnstone, R., and Anderson, E. (2000). Understanding the resistivities observed in geothermal systems. In: Proceedings World Geothermal Congress 2000, Kyushu-Tohoku, Japan, pages pp. 1915–1920.

Verdel, A., Wedemeijer, H., Paap, B., Vandeweijer, V., Weemstra, C., Jousset, P., Franke, S., Blanck, H., Ágústsson K., and Hersir, P. (2016). Reykjanes ambient noise reflection interferometry. Extended abstract EGC, Strasbourg, September 2016.

Wadati, K. (1933). On travel time of earthquake waves. Geophys. Mag., 7:101–111.

Weemstra, C., A., Obermann, A., Verdel, B., Paap, H. Blanck, E. Á. Guðnason, G. P. Hersir, P. Jousset, Ó. Sigurðsson (2016). Time-lapse imaging of the Reykjanes geothermal reservoir. Extended abstract EGC, Strasbourg, September 2016.

Weir, N., White, R., Brandsdóttir, B., Einarsson, P., Shimamura, H., and Hajime, H. (2001). Crustal structure of the northern Reykjanes Ridge and Reykjanes Peninsula, southwest Iceland. Journal of Geophysical Research, 106:6347–6368.

White, R., Bown, J., and Smallwood, J. (1992). Oceanic crustal thickness from seismic measurements and rare earth element inversions. J. Geophys. Res., 97:19,683–19,715.

Zindler, A., Hart, S., Frey, F., and Jakobsson, S. (1979). Nd and Sr isotope ratios and rare earth element abundances in Reykjanes Peninsula basalts evidence for mantle heterogenety beneath Iceland. Earth and Planetary Science Letters, 45:249–262.